Japanese Journal of Applied Physics

The Japan Society of Applied Physics

Investigation of the Low-Frequency Noise Behavior and Its Correlation with the Subgap Density of States and Bias-Induced Instabilities in Amorphous InGaZnO Thin-Film Transistors with Various Oxygen Flow Rates

To cite this article: Chan-Yong Jeong *et al* 2012 *Jpn. J. Appl. Phys.* **51** 100206

View the article online for updates and enhancements.

Related content

- Impact of High-*k* HfO_2 Dielectric on the Low-Frequency Noise Behaviors in Amorphous InGaZnO Thin Film Transistors
  Jae Chul Park, Sun Il Kim, Chang Jung Kim et al.
- Impact of the Use of Xe on Electrical Properties in Magnetron-Sputtering Deposited Amorphous InGaZnO Thin-Film Transistors
  Tetsuya Goto, Shigetoshi Sugawa and Tadahiro Ohmi
- AC Stress-Induced Degradation of Amorphous InGaZnO Thin Film Transistor Inverter
  Dae-Hwan Kim, Dongsik Kong, Sungchul Kim et al.

Recent citations

- Effects of oxygen flow rate on the electrical stability of zinc oxynitride thin-film transistors
  Dae-Hwan Kim *et al*
- Low-frequency noise in amorphous indium–gallium–zinc oxide thin-film transistors with an inverse staggered structure and an SiO_2 gate insulator
  Jae Chul Park and Ho-Nyeon Lee

This content was downloaded from IP address 143.248.110.56 on 26/11/2019 at 09:04

Japanese Journal of Applied Physics **51** (2012) 100206 **RAPID COMMUNICATION**
http://dx.doi.org/10.1143/JJAP.51.100206

Investigation of the Low-Frequency Noise Behavior and Its Correlation with the Subgap Density of States and Bias-Induced Instabilities in Amorphous InGaZnO Thin-Film Transistors with Various Oxygen Flow Rates

Chan-Yong Jeong[1], Ick-Joon Park[1], In-Tak Cho[2], Jong-Ho Lee[2], Euo-Sik Cho[3], Min Ki Ryu[4], Sang-Hee Ko Park[4], Sang-Hun Song[1], and Hyuck-In Kwon[1*]

[1] *School of Electrical and Electronics Engineering, Chung-Ang University, Seoul 156-756, Korea*
[2] *School of Electrical Engineering and Computer Science, Seoul National University, Seoul 151-742, Korea*
[3] *Department of Electronic Engineering, Gachon University, Gyeonggi-do 461-701, Korea*
[4] *Transparent Electronics Team, Electronics and Telecommunications Research Institute, Daejeon 305-700, Korea*

Received May 21, 2012; accepted July 22, 2012; published online October 1, 2012

The low-frequency noise (LFN) behavior and its correlation with the subgap density of states (DOSs) and bias-induced instabilities are investigated in the amorphous indium–gallium–zinc–oxide (a-IGZO) thin-film transistors (TFTs) with various oxygen flow rates. Higher LFN is measured in the higher oxygen flow rate devices in the subthreshold regime, which is attributed to the increased trapping/release processes. We also obtain higher subgap DOSs and larger threshold voltage shifts under positive bias stresses in higher oxygen flow rate devices, which represents that the LFN measured in the subthreshold regime is deeply correlated with the subgap DOSs and electrical instabilities in a-IGZO TFTs. © 2012 The Japan Society of Applied Physics

Since the first report by Nomura,[1)] amorphous indium–gallium–zinc–oxide (a-IGZO) thin-film transistors (TFTs) have been attracting much attention due to their lots of merits including the high mobility, excellent on/off ratio, high uniformity, and low fabrication temperature. Among the various electrical properties of the transistors, low-frequency noise (LFN) is a very important one because it is very sensitive to the electrical traps in electronic devices. Because of this sensitivity, LFN has been used as a simple and complementary diagnostic tool for interface or bulk traps in electronic devices. Recently, a few papers have been published on the LFN behaviors in a-IGZO TFTs.[2–5)] However, most of the works have focused on the investigation of the LFN behavior itself in a-IGZO TFTs, and very few studies[5)] have been made about the correlation of LFN behaviors with the subgap density of states (DOSs) or bias-induced instabilities in a-IGZO TFTs. In this paper, we investigate the LFN behaviors, subgap DOSs, and positive bias-induced instabilities in a-IGZO TFTs with various oxygen flow rates during the channel layer deposition, and observe the relations between the LFNs and other properties.

Figure 1(a) shows the schematic cross-sectional view of the fabricated top gate a-IGZO TFT. The fabrication procedure is as follows: An alkaline-free glass was used as a substrate, and the ultrasonic cleaning process was carried out with acetone, isopropyl alcohol, and deionized water in sequence. The source/drain electrodes were constituted with 150-nm-thick indium tin oxide (ITO), respectively. The a-IGZO active layer was deposited by RF (13.56-MHz) magnetron sputtering using an IGZO target ($In_2O_3 : Ga_2O_3 : ZnO = 1 : 1 : 2$ mol %). The sputtering process was carried out at room temperature in the Ar/O_2 (90/10, 80/20, 70/30 at. %) mixed-gas atmosphere. The thickness of the a-IGZO active layer was 30 nm. All patterning processes were achieved with the photolithographic method and the wet etching process. The gate insulator of 185-nm-thick Al_2O_3 was formed by the atomic layer deposition method at 150 °C. The gate electrode was formed with 150-nm-thick ITO. Finally, devices were subjected to the thermal annealing at 300 °C for 2 h in N_2 ambient. The LFN properties were investigated by measuring the drain current noise power spectral density (S_{ID}) as a function of frequency using a SR570 low-noise current amplifier and a Hewlett Packard 89441A vector signal analyzer. The gate-to-source voltage (V_{GS}) and drain-to-source voltage (V_{DS}) were kept constant during the noise measurements. Figure 1(b) depicts the transfer curves of a-IGZO TFTs with various oxygen flow rates (10, 20, 30%) with a channel width/length (W/L) of 20 μm/20 μm. The data shows that the device with a lower oxygen flow rate has a lower turn-on voltage. In a-IGZO materials, the oxygen vacancy is the source of the electron generation, so the high oxygen pressure during the thin-film deposition reduces the number of electrons.[6)] Because the large number of electrons makes it difficult to turn-off the device, the turn-on voltage moves to the negative direction when the oxygen pressure is low during the thin-film deposition.

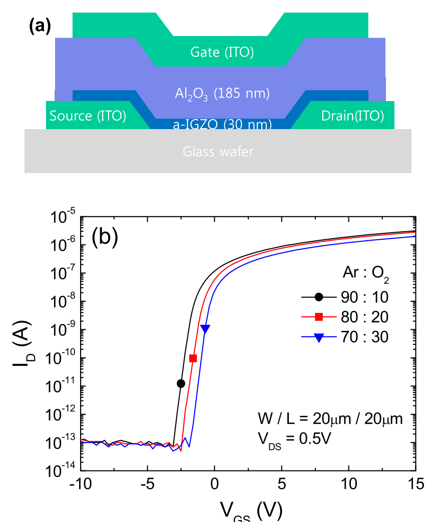

Fig. 1. (Color online) (a) Cross-sectional view of the fabricated a-IGZO TFT. (b) Transfer curves of a-IGZO TFTs with various oxygen flow rates (10, 20, 30%) measured at a V_{DS} of 0.5 V.

*E-mail address: hyuckin@cau.ac.kr

 © 2012 The Japan Society of Applied Physics

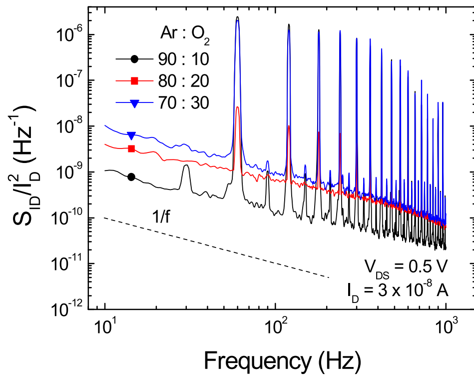

Fig. 2. (Color online) S_{ID}/I_D^2 for devices with various oxygen flow rates measured at the same drain current of 0.03 μA in the subthreshold regime. The large peaks in the figure are due to the 60 Hz noise.

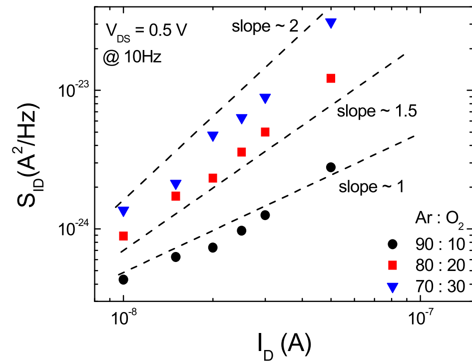

Fig. 3. (Color online) S_{ID} versus I_D at a fixed frequency of 10 Hz measured in the subthreshold regime for a-IGZO TFTs with various oxygen flow rates (10, 20, 30%).

Figure 2 shows the normalized drain current noise spectral density (S_{ID}/I_D^2) for devices with various oxygen flow rates, measured at the same drain current of 0.03 μA in the subthreshold regime. Previously, Kim *et al.* measured the LFN of the a-IGZO TFTs in the linear regime, and tried to correlate the measured LFN with the extracted subgap DOSs.[5] Although this previous work is meaningful, the conclusion still needs to be further considered, because the generation mechanism of the increased LFN in higher subgap DOS devices were ascribed to the bulk mobility fluctuation based on the previous LFN theories[7–10] in this previous work. Considering that the subgap DOS is mainly related with the carrier trapping/release effects and the carrier number fluctuation phenomenon, this results need to be reconsidered. In our experiment, the LFN was mainly observed in the subthreshold regime to correlate the LFN to the subgap DOSs more effectively. In amorphous oxide TFTs, the carrier transport is mainly controlled by multiple trapping and release events when the Fermi level (E_F) resides within the localized tail states inside the bandgap, but the percolation conduction becomes predominant as the E_F moves up to the higher electron energy level than the conduction band edge.[11] Considering that E_F is mainly located inside the bandgap during the subthreshold regime, the subthreshold regime can be more effective than the linear or saturation regime in the correlation of the LFN to the subgap DOSs in amorphous oxide TFTs. The results in Fig. 2 show that the S_{ID}/I_D^2s fit well to a $1/f^a$ power law with $a = 0.9$–1.0 in all devices in the frequency range of 10 Hz to 1 KHz, and the S_{ID}/I_D^2 becomes higher as the oxygen flow rate increases. It represents that the higher oxygen flow rate during the channel deposition cause the increase of subthreshold LFN in a-IGZO TFTs.

Figure 3 depicts the S_{ID} versus I_D measured at a fixed frequency of 10 Hz. According to the previous LFN theories,[7–10] the slope in the S_{ID} versus I_D plot can be used to estimate the dominant LFN generation mechanism in the subthreshold regime. In the carrier number fluctuation model (ΔN) and the correlated number and mobility fluctuation model (ΔN-$\Delta\mu$), the S_{ID} in the subthreshold regime can be expressed as[9]

$$S_{ID} = \frac{q^4}{kT}\frac{N_T}{WLf\gamma C_i^2\eta^2}I_D^2, \qquad (1)$$

$$S_{ID} \propto \frac{kT}{q}\frac{1}{WLf}I_D^2, \qquad (2)$$

where q is the elementary charge, k is the Boltzmann constant, T is the temperature, N_T is the density per unit energy of the dielectric trap in the vicinity of the E_F, γ is the tunneling parameter of the traps and $\lambda = 1/\gamma$ is the tunneling attenuation distance, C_i is the dielectric capacitance per unit area, and η is the parameter which can be obtained from the subthreshold slop (S): $S = (\ln 10)\eta(kT/q)$. For both models, we notice that the S_{ID} follows the quadratic variations versus I_D in the subthreshold regime. However, in the mobility fluctuation model ($\Delta\mu$), the S_{ID} in the subthreshold regime can be expressed as[10]

$$S_{ID} = 2\mu kT\frac{\alpha_H W C_i}{fL^3}\left[1 - \exp\left(\frac{-qV_{DS}}{\eta kT}\right)\right]^{-1} I_D, \qquad (3)$$

where μ is the carrier mobility, and α_H is the Hooge's constant. Equation (3) represents that S_{ID} should have a linear relationship with I_D when $\Delta\mu$ is the dominant LFN generation mechanism in the subthreshold regime.

In Fig. 3, we can observe that the slope in the S_{ID} versus I_D plot progressively changes from ~1 to ~2 as the oxygen flow rate increases during the channel deposition, which shows that the dominant LFN generation mechanism in the subthreshold regime changes from $\Delta\mu$ to ΔN or ΔN-$\Delta\mu$ with the increase of oxygen flow rate in a-IGZO TFTs. Considering that both of ΔN and ΔN-$\Delta\mu$ are caused from the carrier trapping and release processes in the trap states, the results in Fig. 3 represent that the increase of the LFN in the subthreshold regime is mainly due to the increased trap states in higher oxygen flow rate devices.

In order to confirm our assumption, we extracted the subgap DOSs using the differential ideality factor technique[12] in a-IGZO TFTs with various oxygen flow rates. Figure 4(a) shows the extracted subgap DOSs in each device, which shows that both of deep and tail states are highest in the high oxygen flow rate (30%) device, and lowest in the low oxygen flow rate (10%) device. This phenomenon is believed to be caused by the more severe ion bombardment during the sputtering in higher oxygen flow rate environment.[13,14] The obtained result is consistent with the suggested LFN increase

 © 2012 The Japan Society of Applied Physics

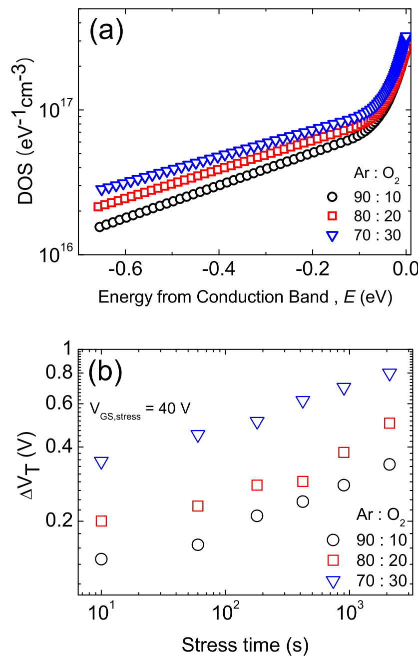

Fig. 4. (Color online) (a) Extracted subgap DOSs in a-IGZO TFTs with various oxygen flow rates (10, 20, 30%). (b) Time dependence of ΔV_T under the application of constant gate bias-stress of 40 V at room temperature in a-IGZO TFTs with various oxygen flow rates (10, 20, 30%).

mechanism in higher oxygen flow rate devices in Fig. 3, and shows that the LFN in the subthreshold regime is deeply correlated with the subgap DOSs in a-IGZO TFTs. Figure 4(b) depicts the time dependence of the threshold voltage shift (ΔV_T) under the application of constant gate bias-stress of 40 V at room temperature. The largest movement of V_T (0.80 V) is observed in the device with a high oxygen flow rate (30%), but the device with a low oxygen flow rate (10%) exhibits the smallest ΔV_T (0.34 V) after inducing the bias-stresses for 2.1×10^3 s. Considering that the charge trapping has been known as the dominant ΔV_T mechanism in a-IGZO TFTs,[15,16] this results can be attributed to the increased subgap DOSs in the high oxygen flow rate device, and are also consistent with the LFNs measured in the subthreshold regime.

In this letter, the LFN behaviors of the a-IGZO TFTs with various oxygen flow rates were investigated in the subthreshold regime, and the correlation was observed between LFNs and other important electrical parameters of the subgap DOSs and positive bias-induced ΔV_Ts. We find that the magnitude of the LFN increases and the slope in the S_{ID} versus I_D plot progressively changes from ~1 to ~2 as the oxygen flow rate increases during the channel deposition in a-IGZO TFTs. Based on the previous LFN theories, we concluded this phenomenon as a result of the increased carrier trapping and release processes due to the increased trap states inside the a-IGZO active layer in higher oxygen flow rate devices. Higher subgap DOSs and larger ΔV_T under the positive bias stresses were also observed in higher oxygen flow rate devices, which shows that the LFN measured in the subthreshold regime is deeply correlated with the subgap DOSs and electrical instabilities of the devices, and the LFN in the subthreshold regime can be an effective diagnosis tool of these properties in a-IGZO TFTs.

Acknowledgement This research was supported by the Chung-Ang University Research Scholarship Grants in 2011.

1) K. Nomura, H. Ohta, A. Takagi, T. Kamiya, M. Hirano, and H. Hosono: Nature **432** (2004) 488.
2) J.-M. Lee, W.-S. Cheong, C.-S. Hwang, I.-T. Cho, H.-I. Kwon, and J.-H. Lee: IEEE Electron Device Lett. **30** (2009) 505.
3) T.-C. Fung, G. Baek, and J. Kanicki: J. Appl. Phys. **108** (2010) 074518.
4) S. Jeon, S. I. Kim, S. Park, I. Song, J. Park, S. Kim, and C. Kim: IEEE Electron Device Lett. **31** (2010) 1128.
5) S. Kim, Y. Jeon, J.-H. Lee, B. D. Ahn, S. Y. Park, J.-H. Park, J. H. Kim, J. Park, D. M. Kim, and D. H. Kim: IEEE Electron Device Lett. **31** (2010) 1236.
6) H. Q. Chiang, B. R. McFarlane, D. Hong, R. E. Presley, and J. F. Wager: J. Non-Cryst. Solids **354** (2008) 2826.
7) G. Reimbold: IEEE Trans. Electron Devices **31** (1984) 1190.
8) K. K. Hung, P. K. Ko, C. Hu, and Y. C. Cheng: IEEE Trans. Electron Devices **37** (1990) 654.
9) D. Rigaud, M. Valenza, and J. Rhayem: IEE Proc.—Circuits Devices Syst. **149** (2002) 75.
10) M. Valenza, A. Hoffmann, D. Sodini, A. Laigle, F. Martinez, and D. Rigaud: IEE Proc.—Circuits Devices Syst. **151** (2004) 102.
11) S. Lee, K. Ghaffarzadeh, A. Nathan, J. Robertson, S. Jeon, C. Kim, I.-H. Song, and U.-I. Chung: Appl. Phys. Lett. **98** (2011) 203508.
12) M. Bae, D. Yun, Y. Kim, D. Kong, H. K. Jeong, W. Kim, J. Kim, I. Hur, D. H. Kim, and D. M. Kim: IEEE Electron Device Lett. **33** (2012) 399.
13) P. Barquinha, L. Pereira, G. Gonçalves, R. Martins, and E. Fortunato: J. Electrochem. Soc. **156** (2009) H161.
14) W.-S. Kim, Y.-K. Moon, S. Lee, B.-W. Kang, K.-T. Kim, J.-H. Lee, J.-H. Kim, B.-D. Ahn, and J.-W. Park: Jpn. J. Appl. Phys. **49** (2010) 08JF02.
15) J.-M. Lee, I.-T. Cho, J.-H. Lee, and H.-I. Kwon: Appl. Phys. Lett. **93** (2008) 093504.
16) M. E. Lopes, H. L. Gomes, M. C. R. Medeiros, P. Barquinha, L. Pereira, E. Fortunato, R. Martins, and I. Ferreira: Appl. Phys. Lett. **95** (2009) 063502.

 © 2012 The Japan Society of Applied Physics